



Magnetism and temperature dependence of nano-TiO₂:Fe EPR spectra

L.S. Molochnikov^a, K.I. Borodin^{b,c}, A.E. Yermakov^{b,c}, M.A. Uimin^{b,c}, A.S. Minin^{b,c,*}, A. V. Vostroknutova^e, R.M. Eremina^e, M.I. Kurkin^b, S.F. Konev^b, A.S. Konev^{b,c}, A. M. Murzakayev^{c,d}, V.S. Gaviko^{c,d}

^a Ural State Forest Engineering University, Yekaterinburg, 620100, Russia

^b M. N. Mikheev Institute of Metal Physics, Ural Branch of the Russian Academy of Sciences, Yekaterinburg, 620108, Russia

^c Ural Federal University, Yekaterinburg, 620002, Russia

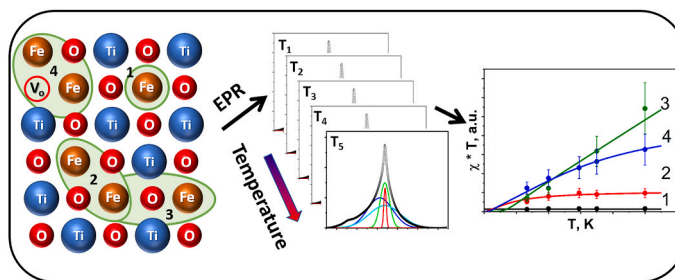
^d Institute of Electrophysics, Ural Branch of the Russian Academy of Sciences, Yekaterinburg, 620016, Russia

^e Zavoisky Physical-Technical Institute, Federal Research Center "Kazan Scientific Center of RAS", Kazan, 420029, Russia

HIGHLIGHTS

- EPR spectra of nano-TiO₂:Fe display a heterogeneous magnetic state.
- Decomposition of EPR signals provides information on different magnetic states of iron ions.
- The anisotropic contribution is negligible compared to the value of the exchange interaction.

GRAPHICAL ABSTRACT



ARTICLE INFO

Keywords:

TiO₂
Temperature dependent EPR
Nanoparticles
AFM-dimers

ABSTRACT

Nanocrystalline TiO₂ samples of various compositions (up to 5 at.% Fe) with anatase structure and an average particle size of about 20 nm were synthesized using sol-gel technology. The magnetic properties of nano-TiO₂:Fe was studied by electron paramagnetic resonance (EPR) and Faraday balance. The existence of an inhomogeneous magnetic state in TiO₂:Fe samples of different compositions were revealed by EPR spectroscopy in a wide temperature range. The analysis of the EPR spectra in the L-, X- and Q-bands allowed us to calculate the quadratic fine structure (D, E) parameters, "axial" and "rhombic" ones, respectively. The value of D turned out to be quite small, which indicates an insignificant anisotropy, which can be ignored describing the magnetic properties of TiO₂:Fe. It was shown that the temperature behavior of different separate components of the integral EPR spectra can be qualitatively interpreted in the model of coexistence in the TiO₂:Fe system, mainly, dimers with a strong negative exchange interaction and isolated paramagnetic centers. No ferromagnetic state in TiO₂:Fe-based samples after etching of aE-prepared state were detected.

* Corresponding author. M. N. Mikheev Institute of Metal Physics, Ural Branch of the Russian Academy of Sciences, Yekaterinburg, 620108, Russia.

E-mail address: calamatica@gmail.com (A.S. Minin).

<https://doi.org/10.1016/j.matchemphys.2021.125327>

Received 15 June 2021; Received in revised form 23 September 2021; Accepted 4 October 2021

Available online 9 October 2021

0254-0584/© 2021 Elsevier B.V. All rights reserved.

1. Introduction

TiO₂-based magnetic semiconductors in the nanocrystalline state are promising materials for different applications such as spintronics, photocatalysts and sensors [1–3]. Of particular interest is the study of the magnetic state of semiconductors doped with 3d metals. However, the nature of magnetism in 3d-doped semiconductors, for example, TiO₂, ZnO, In₂O₃, SnO₂, are still the subject of hot discussions [4,5].

One of the powerful methods that can provide information about the magnetic state of Fe³⁺ ions and other paramagnetic centers is EPR spectroscopy. From the earlier EPR investigations of TiO₂: Fe samples [6], it followed that the spectrum can be described by several lines: narrow intense central peaks and other few lines with a width more than 1000 Oe. These features of EPR spectra were revealed earlier, for example, in works on glasses [7] and α -Al₂O₃ oxide [8] doped with iron and were caused by the clustering of Fe³⁺ ions. The measuring temperature dependencies of EPR signals allows to provide the additional information about the nature of magnetic state and interaction in TiO₂: Fe system, including analysis of single-ion anisotropy.

Thus, the important issue of the work is to analyze the temperature dependence of the separate contributions of multicomponent EPR spectra of TiO₂: Fe samples with different iron content to clarify the role of Fe–Fe interaction at formation of magnetic properties.

2. Methods

Sol-gel method was used to obtain the TiO₂ doped Fe nanoparticles with an anatase structure [6]. An average particle size was about 20 nm. In order to remove the extraneous phases, all samples were etched in 2 M hydrochloric acid at room temperature. Etching treatment is described in detail also in Ref. [6]. The magnetic state of TiO₂: Fe samples (Fe content till E–0.02 at.% Fe, E–0.67% and E–4.7 at.% Fe) in aE-prepared state and after etching is investigated at different temperature by various methods (Faraday balance) and EPR spectroscopy. The chemical compositions of the studied samples based on TiO₂: Fe after etching in HCl, determined by the inductively coupled plasma method (ICP).

The transmission electron microscope (TEM) (JEM 2100 (JEOL)) was used to determine the morphology of the synthesized compounds before and after etching.

X-ray diffraction studies were carried out in copper radiation by means of an Empyrean Series 2 diffractometer manufactured by PANalytical. To calculate the size of coherent scattering region (CSR) and phase compositions, the HighScore v.4.x software package was used.

The magnetic properties of TiO₂: Fe nanopowders were analyzed using Faraday balance at room temperature in fields of up to 12 kOe.

Electron paramagnetic resonance (EPR) measurements at room temperature in X-band were performed using a Bruker ELEXSYS 580 pulse spectrometer in stationary mode. A powder sample was placed in a special quartz tube of 4 mm diameter. The spectra were registered with a Super High-Q rectangular resonator. The interval of the constant magnetic field B was from 480 to 6000 Oe. The level of microwave power was 4.7 mW and the modulation amplitude was 1 Oe. In order to measure the temperature dependence of EPR signal in the range of 100 K up to 500 K the special flowing gas system was used. The integral spectrum decomposition at definite temperature was obtained by the Origin18 program using the Multiple Peak Fit function.

ESR measurements were performed in a Bruker ELEXSYS E500 CW-spectrometer at X-band ($\nu \approx 9.36$ GHz) and Q-band frequencies ($\nu \approx 34$ GHz) equipped with continuous He-gaE-flow cryostats (Oxford Instruments) covering the temperature range 4.2–300 K. ESR spectra

display the power P absorbed by the sample from the transverse magnetic microwave field as a function of the static magnetic field H. The signal-to-noise ratio of the spectra is improved by recording the derivative dP/dH using lock-in technique with field modulation. ESR measurements were performed in a Bruker ELEXSYS E540L -spectrometer at L-band ($\nu \approx 1.0$ GHz).

3. Experimental results and discussion

3.1. X-ray diffraction analysis of samples

The X-ray diffraction of all samples after etching shows that the diffraction lines correspond only the anatase reflections with an almost unchanged lattice parameter $a = 3.794$ Å and $c = 9.504$ Å. In the aE-prepared TiO₂ samples containing of iron less than 4.7 at.% there are no any extraneous phases which could be detected by X-ray analysis. Probably, the absence of another lines means that in the lattice up to 4.7% exist solid solution of Fe in TiO₂. The X-ray diffraction pattern of sample E–0.02 does not differ from the diffraction pattern of sample E–0.67 and E–4.7. The coherent scattering region (CSR) obtained at analysis of X-ray width lines is equal about 20 nm.

3.2. TEM analysis of samples

At transmission electron microscope observation (Fig. 1 (a, b)) it was shown that the particle size of TiO₂: Fe corresponds to the size of CSR of samples E–0.67, E–4.7 defined by X-ray analysis (approximately 20 nm). On the surface of most nanoparticles a disordered nanostructure is observed (see Fig. 1 (a, b) - regions A are shown by arrows). A highly defective interface between adjacent TiO₂ nanoparticles is shown on 1 (b).

It is known that TEM (due to locality of method) and X-ray analysis cannot be able to register the low content of foreign phases, as well as the phases with a small nanoparticle size. That is why all samples, regardless of the X-ray analysis, were subjected to acid treatment to remove all additional phases. So, it allows one to get the samples which contain a solid solution of iron in titanium dioxide lattice without additional phases. To control the magnetic impurities, we used the magnetic analysis of magnetization which is very sensitive to the appearance of ferromagnetic phases independently of particle size.

3.3. Investigation and discussion of magnetic properties

It is known that TEM (due to locality of method) and X-ray analysis cannot be able to register the low content of foreign phases, as well as the phases with a small nanoparticle size. That is why all samples, regardless of the X-ray analysis, were subjected to acid treatment to remove all additional phases. So, it allows one to get the samples which contain a solid solution of iron in titanium dioxide lattice without additional phases. To control the magnetic impurities, we used the magnetic analysis of magnetization which is very sensitive to the appearance of ferromagnetic phases independently of particle size.

The magnetization curves of the E–0.02, E–0.67 and E–4.7 samples at room temperature (RT) can be described by linear functions typically for the paramagnetic state (see Fig. 2). The extrapolation of magnetization curve to zero magnetic field does not show any ferromagnetic contribution.

The same Fig. 2 shows the calculated magnetization curves obtained under the assumption that all Fe³⁺ ions have a magnetic moment corresponding to the spin $S = 5/2$, and their behavior in a magnetic field is described by the Brillouin function, as it should be for noninteracting

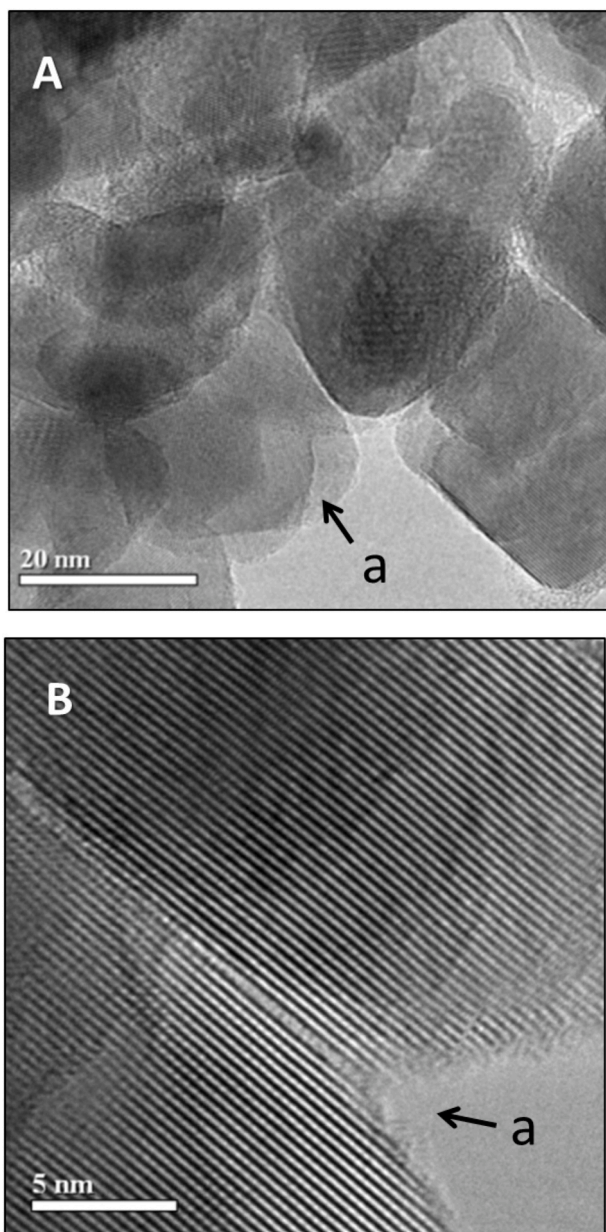


Fig. 1. HRTEM of the initial sample after etching of TiO₂: Fe (a) and the fragment of the sample with boundary (b). Arrows A indicate the disordered regions.

paramagnetic ions. The experimental values of magnetization are noticeably lower than the calculated ones for all three samples. We believe that this is due to negative exchange interactions between iron ions. Different variants of the mutual arrangement of 2 iron ions in the TiO₂ lattice, as well as the possibility of realizing more complex configurations (for example, trimers, etc.) can lead to different values of the exchange parameter J and different contributions to the total magnetization from clusters of Fe³⁺ ions. These contributions cannot be separated using magnetic data alone. An analysis of the intensity and width of individual lines of the EPR spectra can make it possible to distinguish both the contribution from noninteracting paramagnetic centers and from possible clusters of Fe³⁺ ions with different exchange interactions.

When describing magnetic data, one cannot exclude the possible contribution of anisotropy of one nature or another. Using the EPR data, one can estimate the magnitude of the anisotropic contributions by determining the magnitude of the zero-field splitting (zfs) - D . Processing the TiO₂: Fe spectra measured in different ranges (L, X and Q) using

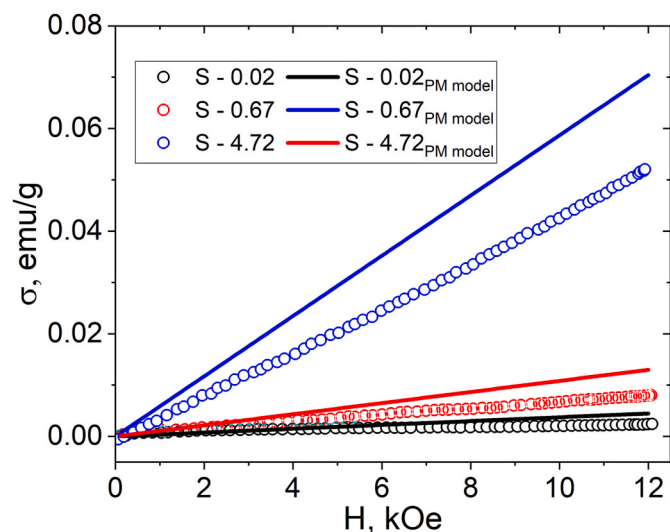


Fig. 2. Magnetization curves of samples at room temperature with different compositions (E=0.02, E=0.67, E=4.7) after etching (solid circles). The dash lines denote the Brillouin functions for all samples (E=0.02, E=0.67, E=4.7).

approaches [9] made it possible to estimate the value of D .

The EPR of Fe³⁺ in compounds can be described by the following spin Hamiltonian, containing only the Zeeman and fine structure terms [9]:

$$\mathcal{H} = g\mu_B BS + DS_z^2 + E(S_z^2 - S_y^2) \quad (1)$$

where g for E-ions is very close to the free-electron g -value $g_e = 2.0023$, $DS_z^2 + E(S_z^2 - S_y^2)$, the terms that determine the fine structure, where $D = \frac{2}{3}D_{zz}$, $E = \frac{1}{2}(D_{xx} - D_{yy})$. Stevens operators are related with the parameters of the crystal field $B_2^0 = \frac{1}{3}D$, $B_2^2 = E$.

Temperature dependence of the ESR spectra at X-band frequency for TiO₂:Fe is shown in Fig. 3. At low temperatures 8 K the ESR line shape can be fitted as the sum of three ESR signals.

Strictly speaking, fitting the EPR signal with only three lines makes it possible to quite rigorously determine only the value of D to explain the appearance of a line with a g -factor of about 4.3. As shown earlier in the work [6], the EPR spectrum should be described by a large number of

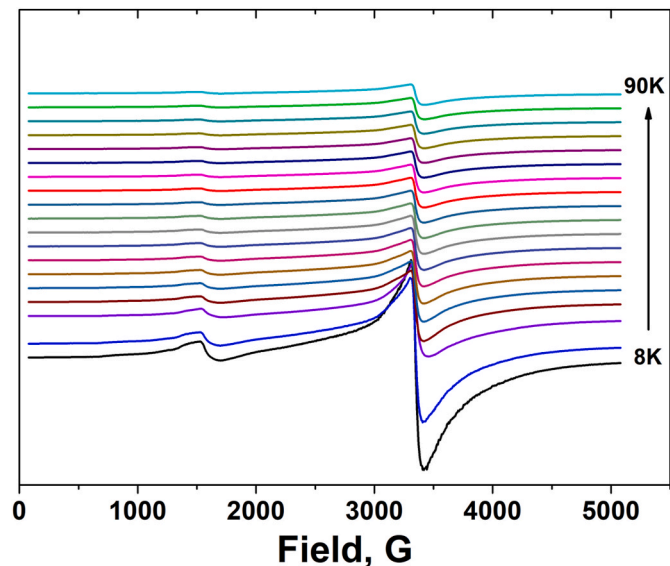


Fig. 3. Temperature dependence of the EPR spectrum of TiO₂: Fe sample in the X-range.

lines - at least five, four of which are located near the g-factor 2. The nature of these lines requires in the future a deeper analysis, taking into account not only the effect of the crystal field, but the exchange interaction between the spins of iron ions. Thus, the proposed fitting in this work is carried out in order to establish the value of D and to explain the appearance of a line with a g-factor of 4.3 in the EPR spectrum.

ESR signal of each paramagnetic center was fitted by the polycrystalline lineshape with g_{\parallel} and g_{\perp} , being a superposition of asymmetric Lorentzian lineshape [10]. The parameters g_{\parallel} and g_{\perp} were determined from the relation $h\nu = g\mu_B H_{res}$, where the resonant value of

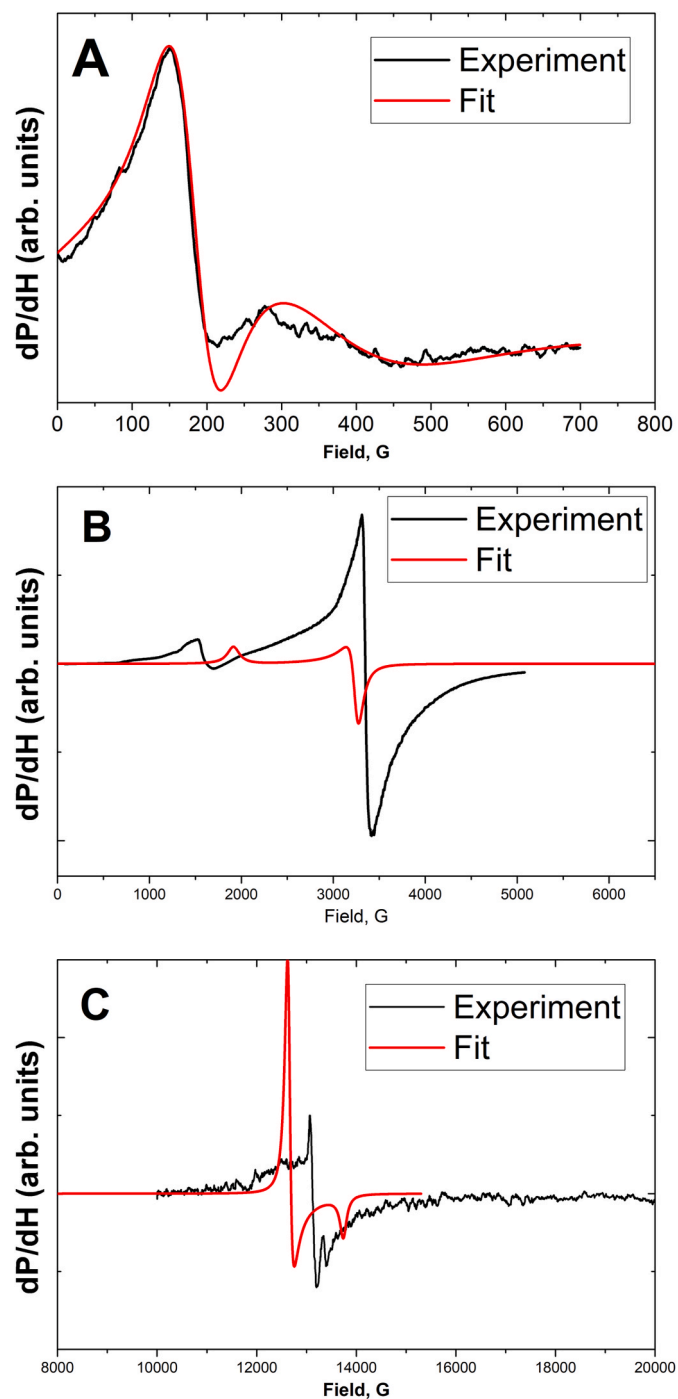


Fig. 4. Theoretically calculated spectra (red line) and experimental for $D = 0.11$ K, $E = -D/3$ for EPR spectra of TiO_2 : Fe sample recorded in the L-(A), X-(B) and Q-ranges (C). (For interpretation of the references to colour in this figure legend, the reader is referred to the Web version of this article.)

the magnetic field H_{res} was determined from the diagonalization of the energy matrix which based on the Hamiltonian (1). The condition for determining the value of the resonant fields was the requirement that the difference between the energy levels and the microwave quantum are equal. ESR signals of each microwave band (L-, X- and Q-) were fitted by the polycrystalline lineshape with g_{\parallel} and g_{\perp} , which were obtained using the matrix (1) for each of the transitions.

To describe the EPR spectra in the L-band, a fitting was performed with the parameters $D = 0.11$ K; $E = -D/3$; $\Delta H_{per} = 80$; $\Delta H_z = 80$; $g_x = g_z = 2$. The same parameters make it possible to describe with reasonable accuracy the experimental EPR spectra in the X- and Q-ranges (see the insets in Fig. 4A and B,C).

The obtained value of D equal to 0.11 K, which explains the appearance of a g-factor of 4.3 in EPR spectra, is a relatively small value in comparison with the value of the exchange J , for example, in dimers (J of the order of (10–100) K), which we previously used [6] to describe the magnetic properties of these systems. In addition, we should note that the relative contribution of the EPR signal with a g-factor of 4.3 to the total integrated signal intensity is several percent.

Thus, for the subsequent description of the magnetic properties of these systems, one can neglect the anisotropy and describe the TiO_2 : Fe system only considering isolated paramagnetic centers and exchange-coupled clusters, in the simplest case, dimers.

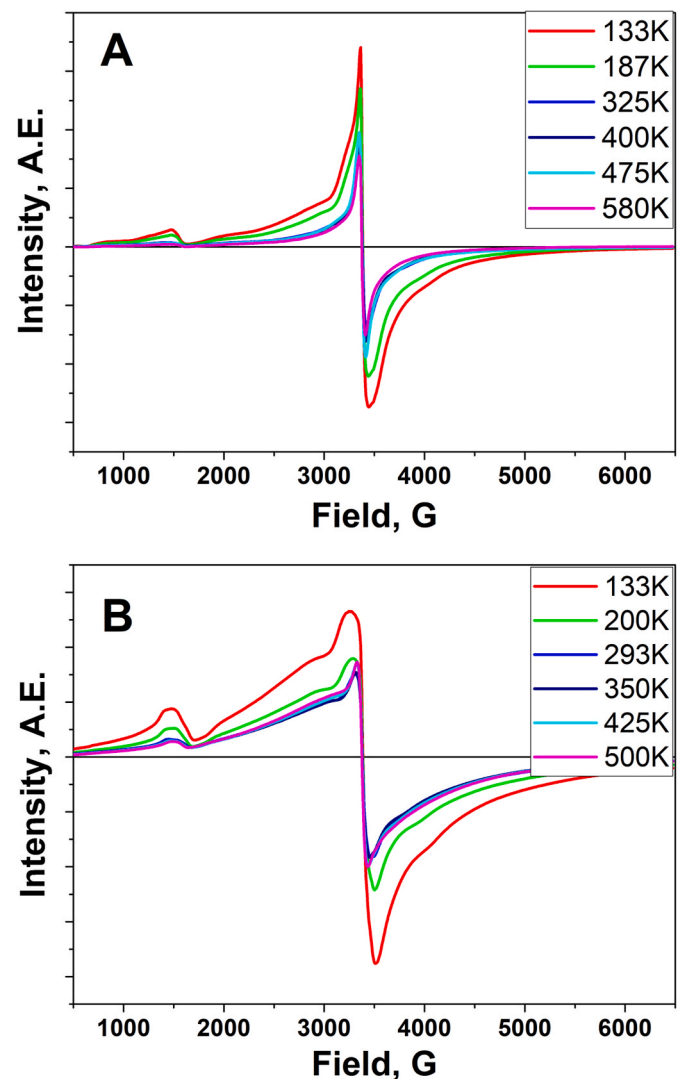


Fig. 5. Decomposition of the experimental EPR integral spectra of sample E-0.67 (a -325 K) and E-4.7 (b-295 K) into 5 spectral components.

3.4. Temperature EPR analysis of TiO₂:Fe samples and discussion

The temperature dependence of the central EPR signal of samples E–0.67 and E–4.7 in the X-range is characterized by a g-factor close to 2 at different T, and besides the shape of the EPR signal of those central lines strongly depends on the iron concentration (Fig. 5 (a,b)).

Except the main signal ($g=2$), the additional lines can be visible and distinguish in the range of fields from 2000 to 3500 Oe. The shape of these lines depends on the concentration of iron in the samples (Fig. 5 (A, B)). A low-intensity line (with a g-factor of about 4.3) is also revealed for both samples E–0.67 and E–4.7, which can be connected with Fe³⁺ in the octahedral positions having rhombohedral distortions [6,11–13] or can be localized at the particle surface. Thus, the spectrum is a combination of different contributions and, can be decomposed into several components (Table 1). We can do it in the paper [6], but without analyzing of temperature dependence of the EPR spectra components.

Fig. 6 (A, B) shows examples of the decomposition of the EPR absorption curves into 5 separate components both for E–0.67 sample and E–4.7 sample at RT. The decomposition into 5 components was carried out under the assumption that there are Gaussian lines which are typical for the nonhomogeneous magnetic systems [14]. The convergence factor (or difference spectrum) between the experimental and calculated cumulative curves for sample E–0.67 is consisting about 0.04%. Attempts to decompose the absorption curve into a smaller number (3 or 4) of components were unsuccessful. Decomposition into 4 components for the same sample E–0.67 led to high difference 7.3% in areas between the experimental and calculated cumulative curve.

The relative integrated intensity of the lines (1–4) of the EPR spectra of samples E–0.67 and E–4.7 is given in the table.

The width and shape of the lines in our case is determined by the dipole and exchange interactions between the magnetic moments of the Fe³⁺ ions. Considering the effects of the crystal field in the presence of structural defects (for example, oxygen vacancies) [15], the exchange interaction can lead not to narrowing, but to broadening of the EPR lines [16]. Experimentally, in the EPR spectra, we observe a relatively narrow line (1) from paramagnetic centers with dipole-dipole interaction and several broad lines (2–4), probably from pairs with exchange interaction.

The widths of each component of the spectra samples E–0.67 and E–4.7 at different temperatures are shown in Fig. S1 and Fig. S4 respectively (Supplement Information). A relatively small change in the width of each line with temperature can be noted. Fig. S3 and Fig. S4 show the temperature variation of the integral intensity (area under the S curve) of each of these lines. Note a rather strong change in the intensity of lines 3 and 4 compared to the intensities of lines 1 and 2. To identify each line, i.e. to assign them to one or another type of carriers of the magnetic moment, we tried to analyze the change in the integral intensity of spectral lines with temperature. The integral intensity of the EPR line is directly proportional to the susceptibility. In our case the relative changes in the susceptibility with temperature are important, so we will use the relative intensity of each line of the EPR spectrum (S) as the value of the susceptibility χ , and denote as χ_{EPR} . At analysis of the temperature dependence of the susceptibility, the experimental results are often presented as the product $\chi \cdot T$ versus T [17] (Fig. 7). For the simplest case - a set of non-interacting moments in accordance with Curie's law, this function will be a constant equal to the Curie constant.

Table 1
Integrated intensity of spectral lines for samples E–0.67 (325 K) and E–4.7 (295 K).

Line number	S1	S2
1	0.045	0.026
2	0.194	0.166
3	0.351	0.390
4	0.327	0.392

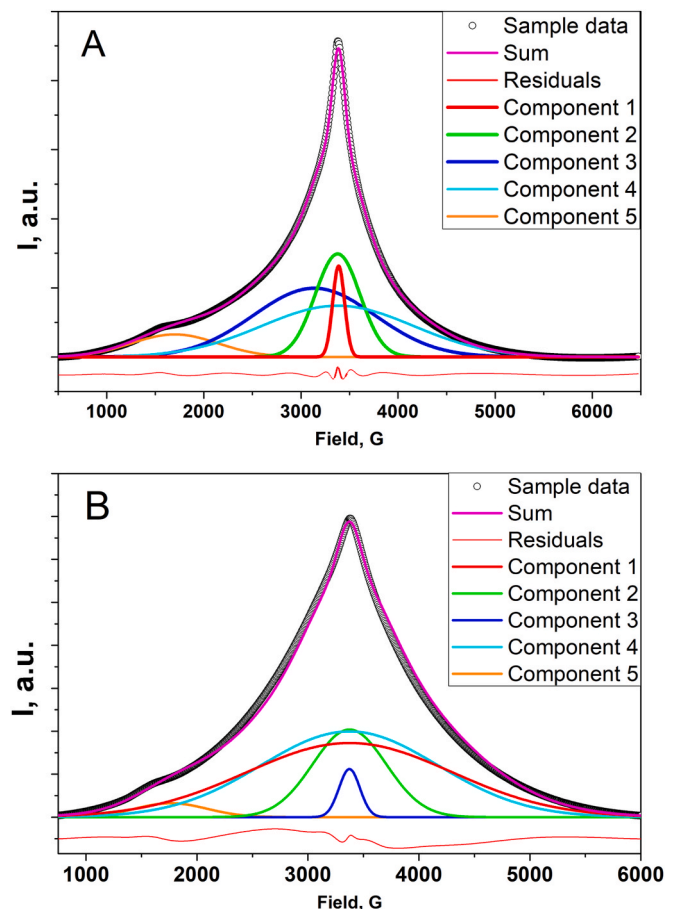


Fig. 6. The EPR spectra of samples E–0.67 (a), E–4.7 (b) are measured in the given temperature range (from 133 K to 580 K (a) and from 133 K to 500 K (b)).

If, in addition to such moments, there is a temperature-independent paramagnetic or diamagnetic contribution, this will be a linear function of temperature with a positive or negative slope, but as T tends to zero, this function should remain positive (the Curie constant is positive by definition).

As noted above, when describing the magnetic properties of TiO₂ doped with iron, we must also consider the formation of exchange-coupled magnetic moments (dimers). The properties of magnetics containing isolated and exchange-coupled moments are presented in Ref. [6] which describes the temperature dependence of the initial magnetic susceptibility of such objects. In figure shows some model functions $\chi \cdot T$ versus T from Ref. [17], reflecting different variants of the temperature behavior of non-interacting and interacting paramagnetic centers (dimers).

The $\chi \cdot T$ function for non-interacting moment carriers does not depend on temperature. With a relatively small exchange parameter (up to several tens of K), the calculated functions exhibit nonlinear behavior in the temperature range (0–500) K. With an increase in negative exchange to 300 K, only an initial almost linear segment remains in this temperature range. Extrapolating the $\chi \cdot T$ function to the low-temperature region for J = 300 K leads to an intersection with the T-axis near 50 K. This intersection point can serve as a measure of the exchange interaction level in pairs.

In Fig. 7(a and b) shows the experimental dependences $\chi_{\text{EPR}} \cdot T$ versus T for 4 spectral components of samples E–0.67 and E–4.7, obtained as a result of the decomposition of the integral spectra of the

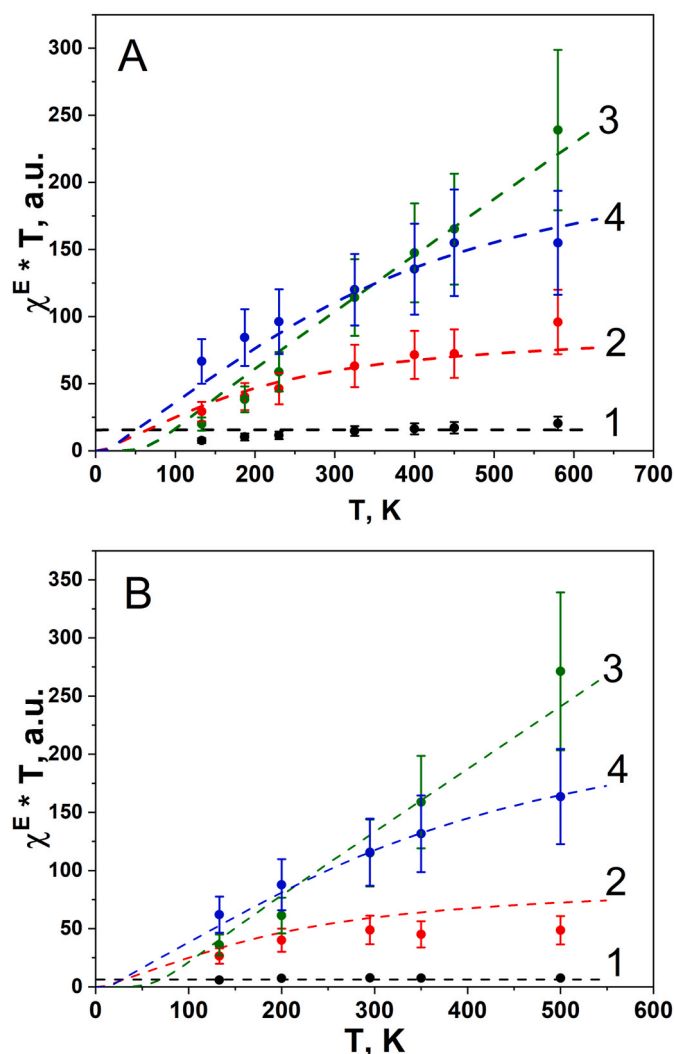


Fig. 7. Decomposition of the experimental EPR integral spectra of sample E-0.67 (a –325 K) and E-4.7 (b-295 K) into 5 spectral components.

corresponding samples.

We tried to describe these temperature dependences on the basis of the concepts developed in Ref. [13], varying the value of exchange in pairs in order to obtain the closest agreement between experiment and theory.

Fig. 7(a and b) (a, b) demonstrate that the $\chi_{EPR} \cdot T$ value for component 1 (non-interacting Fe^{3+} ions) does not depend on temperature in complete agreement with theory. The experimental data $\chi_{EPR} \cdot T$ versus T components of the spectra (2–4) are satisfactorily described by the calculated functions for dimers with negative exchange interactions of different values. The dependence $\chi_{EPR} \cdot T$ versus T for component 3 requires the largest exchange value for the description - about 300 K. Components 2 and 4 are described by theoretical functions $\chi \cdot T$ with exchange of 40 and 70 K, respectively.

Thus, a qualitative analysis of the $\chi_{EPR} \cdot T$ versus temperature allows one to obtain the information about the magnetic contributions of different nature existing in the system of iron magnetic moments in the TiO_2 matrix. This analysis confirms the previous assumption about the coexistence in the system of isolated paramagnetic centers and clusters (presumably, Fe^{3+} - Fe^{3+} dimers) with a significant negative exchange

interaction.

4. Conclusion

The temperature dependence of the separate components in the complex EPR spectra for $TiO_2:Fe$ samples display the different magnetic contributions. Some components (lines widths do not exceed 450 Oe) exhibit behavior close to the Curie law, which can be attributed to isolated paramagnetic centers or centers with a weak dipole-dipole interaction. Other components (lines width is more than 1000 Oe) demonstrate more complicated temperature dependence (CW) and indicate that the system has dominant strong negative exchange interactions, which can relate to Fe clusters or dimers in the TiO_2 matrix. The value of the anisotropic contributions in describing the magnetic properties of the $TiO_2:Fe$ system is negligible. It should be underlined that in $TiO_2:Fe$ samples (with Fe content up to 4.7 at.%) after etching no ferromagnetic contribution was detected.

CRediT authorship contribution statement

L.S. Molochnikov: Conceptualization, Investigation, (EPR), Writing – original draft. **K.I. Borodin:** Investigation, (EPR), Formal analysis. **A. E. Yermakov:** Conceptualization, Methodology, Supervision, Writing – original draft. **M.A. Uimin:** Writing – original draft, Funding acquisition. **A.V. Vostroknutova:** Investigation, (EPR). **R.M. Eremina:** Investigation, (EPR), Methodology, Writing – original draft. **M.I. Kurkin:** Methodology. **S.F. Konev:** Investigation, (EPR). **A.S. Konev:** Investigation, (EPR), Data curation. **A.M. Murzakayev:** Formal analysis, Software, Visualization, Investigation, (TEM). **V.S. Gaviko:** Investigation, (XRD).

Declaration of competing interest

The authors declare that they have no known competing financial interests or personal relationships that could have appeared to influence the work reported in this paper.

Acknowledgement

This work was carried out within the framework of the state task of the Russian Ministry of Education and Science (subject “Magnet”, state registration number AAAA-A18-118020290129-5, “Quant” state registration number AAAA-A18-118020190095-4 and subject “Alloys” state registration number AAAA-A19-119070890020-3) and also with partial support from the RFBR grant (project No. 20-02-00095a). We are especially grateful to A.V. Korolev, A.F. Gubkin, and K.N. Mikhalev, employees of the M.N. Mikheev Institute of Metal Physics of Ural Branch of Russian Academy of Sciences for their useful assistance and discussion of the results. We would like to express our gratitude to the Center for Collective Use of the IMP UB RAS for conducting XRD and SQUID studies.

Appendix A. Supplementary data

Supplementary data to this article can be found online at <https://doi.org/10.1016/j.matchemphys.2021.125327>.

References

- [1] Y. Sui, Q. Liu, T. Jiang, Y. Guo, Appl. Surf. Sci. 428 (2018) 1149–1158.
- [2] B. Chen, A.J. Haring, J.A. Beach, M. Li, G.S. Doucette, A.J. Morris, R.B. Moore, S. Priya, RSC Adv. 4 (2014) 18033–18037.

- [3] B.K. Kaleji, S. Mirzaee, S. Ghahramani, S. Rezaie, N. Hosseinabadi, A. Fujishima, *J. Mater. Sci. Mater. Electron.* 29 (2018) 12351–12359.
- [4] L. Pereira, *J. Phys. Appl. Phys.* 50 (2017) 393002.
- [5] J. Coey, M. Venkatesan, P. Stamenov, *J. Phys. Condens. Matter* 28 (2016) 485001.
- [6] A.Y. Yermakov, A.F. Gubkin, A.V. Korolev, L.S. Molochnikov, M.A. Uimin, E. V. Rosenfeld, M.I. Kurkin, A.S. Minin, A.S. Volegov, D.W. Boukhvalov, et al., *J. Phys. Chem. C* 123 (2018) 1494–1505.
- [7] R.S. Chakradhar, A. Murali, J.L. Rao, *Opt. Mater.* 10 (1998) 109–116.
- [8] G. Wertheim, J. Remeika, *Phys. Lett.* 10 (1964) 14–15.
- [9] I. Edelman, J. Kliava, O. Ivanova, R. Ivantsov, D. Velikanov, V. Zaikovskii, E. Petrakovskaja, Y. Zubavichus, S. Stepanov, *J. Non-Cryst. Solids* 506 (2019) 68–79.
- [10] R. Eremina, I. Yatsyk, A. Shestakov, I. Fazlizhanov, T. Gavrilova, F. Milovich, A. Zinnatullin, F. Vagizov, I. Gilmutdinov, P. Shirshnev, et al., *J. Phys. Chem. Solid.* 133 (2019) 7–14.
- [11] T. Berger, M. Sterrer, O. Diwald, E. Knözinger, D. Panayotov, T.L. Thompson, J. T. Yates, *J. Phys. Chem. B* 109 (2005) 6061–6068.
- [12] Z. Barbieriková, D. Dvoranová, M.-V. Sofianou, C. Trapalis, V. Brezová, *J. Catal.* 331 (2015) 39–48.
- [13] M.N. Grecu, S. Constantinescu, D. Tărăbășanu-Mihăilă, D. Ghica, I. Bibicu, *Phys. Status Solidi* 248 (2011) 2927–2931.
- [14] S.A. Al'Tshuler, B.M. Kozyrev, *Electron Paramagnetic Resonance*, Academic Press, 2013.
- [15] M. Horn, C. Schwerdtfeger, *J. Phys. Chem. Solid.* 32 (1971) 2529–2538.
- [16] A. Abragam, B. Bleaney, *Electron Paramagnetic Resonance of Transition Ions*, OUP Oxford, 2012.
- [17] M. Reis, *Fundamentals of Magnetism*, Elsevier, 2013.